nature biotechnology

ARTICLES

https://doi.org/10.1038/s41587-020-0741-7

A long-term study of AAV gene therapy in dogs with hemophilia A identifies clonal expansions of transduced liver cells

Giang N. Nguyen[1,8], John K. Everett[2,8], Samita Kafle[1], Aoife M. Roche[2], Hayley E. Raymond[2], Jacob Leiby[2], Christian Wood[1], Charles-Antoine Assenmacher[3], Elizabeth P. Merricks[4,5], C. Tyler Long[4,5], Haig H. Kazazian[6], Timothy C. Nichols[4,5], Frederic D. Bushman[2] and Denise E. Sabatino[1,7] ✉

Nine dogs with hemophilia A were treated with adeno-associated viral (AAV) gene therapy and followed for up to 10 years. Administration of AAV8 or AAV9 vectors expressing canine factor VIII (AAV-cFVIII) corrected the FVIII deficiency to 1.9–11.3% of normal FVIII levels. In two of nine dogs, levels of FVIII activity increased gradually starting about 4 years after treatment. None of the dogs showed evidence of tumors or altered liver function. Analysis of integration sites in liver samples from six treated dogs identified 1,741 unique AAV integration events in genomic DNA and expanded cell clones in five dogs, with 44% of the integrations near genes involved in cell growth. All recovered integrated vectors were partially deleted and/or rearranged. Our data suggest that the increase in FVIII protein expression in two dogs may have been due to clonal expansion of cells harboring integrated vectors. These results support the clinical development of liver-directed AAV gene therapy for hemophilia A, while emphasizing the importance of long-term monitoring for potential genotoxicity.

Gene therapy for hemophilia A has moved from preclinical studies in mice and dogs to successful trials in humans[1–4]. AAV vectors to deliver the factor VIII gene (*F8*) were first evaluated in dogs with hemophilia A in the early 2000s[5–7]. While AAV gene therapy has demonstrated promising results for hemophilia B in clinical studies for more than 8 years[8,9], studies for hemophilia A are at an earlier stage[1–4]. As recombinant (r)AAV commonly persists in an episomal form[10], rAAV may not be maintained in tissues undergoing cell division. However, as hepatocytes in healthy dogs are typically quiescent[11], the dog model is well suited to long-term studies designed to understand the durability and safety of AAV gene therapy and to evaluate tissues that are not accessible in human patients.

One of the safety concerns for AAV gene therapy is the potential for genotoxic integration events. After introduction into cells, rAAV primarily remains episomal[10], but integration into the host genome has been observed in mice[12–16], non-human primates[17] and humans[17,18]. To date, there have been no serious adverse events involving genotoxicity as a result of rAAV vector integration in humans or large animals. Other studies of wild-type AAV in humans or rAAV in mouse models have detected tumors associated with AAV. Studies of wild-type AAV reported AAV integration events in human hepatocellular carcinoma (HCC), suggesting a possible role of AAV integration in transformation[19–21]. However, the AAV copy number was much less than one per cell, thus the idea that integration events caused HCC seemed unlikely[19–21]. Another study showed that some AAV2 vectors contain a sequence in the 3′ untranslated region, adjacent to the AAV inverted terminal repeat (ITR), that has enhancer-promoter activity in liver cells[22]. This element has been identified in HCC in humans and may be a mechanism of transformation in these tumors[20]. While HCC has not been observed in rAAV-treated adult mice or other mammals[12,17,18,23], the development of rAAV-associated HCC has been reported after delivery to neonatal mice[14,24–26] and to young adults of mouse strains that have a high incidence of spontaneous liver tumors[27,28]. This suggests that active cell division, such as that occurring during development, can be associated with genotoxic integration events[14,24,25]. In neonatal mice, rAAV integration events were identified recurrently in specific genomic regions in HCC tissue, suggesting possible insertional mutagenesis[15]. The above findings warrant further research to assess the safety of rAAV gene therapy.

In this study, we treated nine dogs with hemophilia A with AAV-cFVIII and followed them for as long as 10 years. Levels of cFVIII activity were maintained throughout the study, representing the longest sustained therapeutic levels of FVIII expression observed in a large-animal model of hemophilia A associated with a significant reduction in spontaneous bleeding events. Two dogs showed a gradual increase in FVIII expression levels. Upon termination of the study, AAV integration analysis on the liver tissue of these two dogs and four other dogs revealed clonal expansion of

[1]The Raymond G. Perelman Center for Cellular and Molecular Therapeutics, Children's Hospital of Philadelphia, Philadelphia, PA, USA. [2]Department of Microbiology, Perelman School of Medicine, University of Pennsylvania, Philadelphia, PA, USA. [3]Department of Pathobiology, School of Veterinary Medicine, University of Pennsylvania, Philadelphia, PA, USA. [4]Department of Pathology and Laboratory Medicine, University of North Carolina at Chapel Hill, Chapel Hill, NC, USA. [5]UNC Blood Research Center, University of North Carolina School of Medicine, University of North Carolina at Chapel Hill, Chapel Hill, NC, USA. [6]Department of Genetic Medicine, Johns Hopkins School of Medicine, Baltimore, MD, USA. [7]Division of Hematology, Department of Pediatrics, Perelman School of Medicine, University of Pennsylvania, Philadelphia, PA, USA. [8]These authors contributed equally: Giang N. Nguyen, John K. Everett. ✉e-mail: dsabatin@pennmedicine.upenn.edu

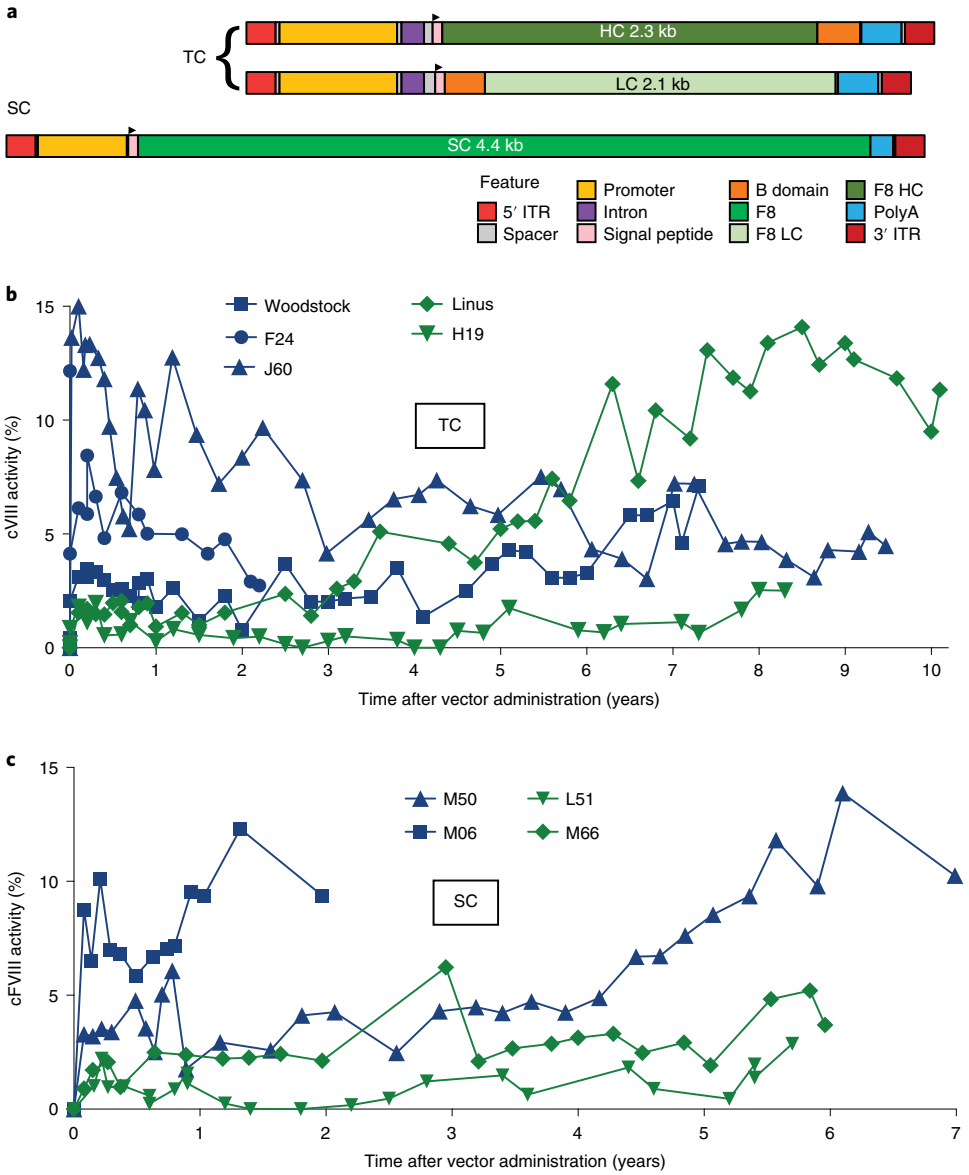

Fig. 1 | Long-term expression of AAV-cFVIII in dogs with hemophilia A. a, Genetic structures of the vectors used, illustrating the TC (top) and SC (bottom) designs. The features of these constructs are indicated by the colors shown in the legend. The TC-delivery approach consisted of co-delivering the 2.3 kb *cF8* HC in one AAV vector and the 2.1 kb *cF8* LC in a second AAV vector. These vectors used the thyroxine-binding globulin (*TBG*) promoter and two copies of α1-microglobulin–bikunin enhancer sequences (695 bp) with an intron (175 bp) for liver-directed gene expression. The construct used a 263 bp SV40 polyA signal. The SC-delivery approach consisted of delivering the 4.4 kb B domain deleted *cF8*, driven by a minimal hepatic control region (192 bp) and the human α-1-antitrypsin (HCR-*hAAT*) promoter (266 bp). This construct included a 134 bp SV40 polyA signal. The gray regions indicate spacers or cloning sites. The TC vector was delivered by portal vein infusion, while the SC vector was delivered by peripheral vein infusion. **b**, Longitudinal quantification of FVIII levels after the TC-delivery approach. In the TC approach, the total AAV dose was 2.5×10^{13} viral genomes (vg) per kg for F24 (AAV8), Woodstock (AAV9) and J60 (AAV9) (blue). Linus (AAV8) and H19 (AAV9) were treated at a low-vector dose (total vector dose of 1.2×10^{13} vg per kg; green). **c**, FVIII levels after the SC-delivery approach. AAV8 delivery of the SC to dogs with hemophilia A was performed using a vector dose of 4×10^{13} vg per kg (M50, M06; blue) and a vector dose of 2×10^{13} vg per kg (L51, M66; green).

cells, with insertions near genes that are associated with cancer in humans, but not overt nodule formation or transformation.

Results

Sustained FVIII expression after AAV delivery. We treated dogs with hemophilia A using two approaches, with either the two *cF8* chains (TC) encoded separately or a single chain (SC) encoded in one vector[6] (Fig. 1a and Table 1). The TC approach takes advantage of the normal intracellular processing of FVIII, in which FVIII undergoes proteolytic cleavage into two polypeptides that form a heterodimer, which is subsequently secreted. In this approach, an AAV vector (AAV8 or AAV9) encoding the *cF8* heavy chain (HC) was co-delivered with an AAV vector encoding the *cF8* light chain (LC)[6]. The SC approach used an AAV8 vector to deliver *cF8* with the B domain deleted[6].

All the AAV-treated dogs with hemophilia A maintained cFVIII expression for the duration of the entire study (2.2–10.4 years; Fig. 1b,c and Table 1). These dogs with hemophilia A have an intron 22 inversion that is analogous to the most common mutation in humans and have a severe bleeding phenotype (<1% cFVIII activity)[29].

Table 1 | Summary of AAV administration, FVIII activity and DNA analysis of dogs with hemophilia A

AAV delivery approach	Total AAV vector dose (vg per kg)[a]	AAV serotype	Dog with hemophilia A	Years evaluated[b]	cFVIII activity (%)		DNA analysis of liver samples			
					Mean ± s.d.	Final	Number of liver samples[c]	Mean VCN per diploid genome ± s.d.	Copy number range	Number of genomic integration sites recovered[d]
TC	2.5×10^{13}	AAV8	F24	2.2	5.7 ± 2.3	2.7	ND[e]	ND	ND	ND
		AAV9	Woodstock	8.2	3.1 ± 1.5	7.1	5	0.28 ± 0.10	0.19–0.42	ND
		AAV9	J60	9.5	8.1 ± 4.0	4.5	29	3.43 ± 2.34	0.76–7.82	271
	1.2×10^{13}	AAV8	Linus	10.1	5.9 ± 4.6	11.3	15	0.28 ± 0.21	0.01–0.62	131
		AAV9	H19	8.3	0.9 ± 0.7	2.5	11	0.17 ± 0.09	0.07–0.33	160
SC	4×10^{13}	AAV8	M06	2.3	7.4 ± 2.6	9.4	8	1.44 ± 0.69	0.37–2.26	764
			M50	7.3	5.2 ± 3.6	10.3	29	0.35 ± 0.34	0.00–1.14	258
	2×10^{13}		L51	6.1	0.8 ± 0.6	1.9	5	0.01 ± 0.02	0.00–0.04	ND
			M66	6.0	2.6 ± 1.3	3.7	13	0.32 ± 0.18	0.00–0.60	161

[a]In the TC-delivery approach, the vector dose was 1.25×10^{13} vg per vector per kg at the high dose and 6×10^{12} vg per vector per kg at the low dose. [b]The number of years after AAV administration. [c]The number of liver samples analyzed in the VCN analysis. [d]Integration studies were performed on three liver samples per dog. [e]ND, not determined.

After AAV administration, the mean levels of cFVIII activity for the dogs treated with the TC approach were 5.6% of normal for the dogs at the high-vector dose and 3.4% for the dogs at the low-vector dose (Table 1). One dog (J60) treated at the high-vector dose required a splenectomy at the time of vector infusion and had a higher level of cFVIII expression (8.1% ± 4.0%) than that of the other dogs treated at this dose (see Methods for additional details). For the SC-treated dogs, the mean levels of cFVIII expression were 6.2% for the high-vector dose and 1.7% for the low-vector dose. At the final time points, all dogs had levels of cFVIII activity that were close to or greater than the mean cFVIII expression (Table 1). FVIII activity was also demonstrated by a shortening of the whole-blood clotting time (Supplementary Fig. 1).

Two dogs (Linus and M50) had a gradual increase in cFVIII expression levels that began more than 4 years after vector administration. Linus had a cFVIII activity of 4% at 4 years after vector delivery, which gradually increased to 11% at 10 years after AAV administration (Fig. 1b). M50 had a cFVIII activity of 4% at 4 years after AAV delivery, which gradually increased to 10% at 7 years after vector administration (Fig. 1c). Two other dogs, Woodstock and M06, also had possible modest increases in FVIII activity levels.

Clinical observations after AAV gene therapy. A cohort of naive dogs with hemophilia A ($n=11$) was followed prospectively for 4 years to determine the frequency of bleeding events. All bleeding events required treatment with recombinant cFVIII[30] or normal canine blood products. The annualized bleeding rate (ABR) was 12.7 ± 6.0 bleeds per year (ref. [31]; Supplementary Fig. 2), similar to the ABR for patients with hemophilia who are treated episodically (18.5 bleeds per patient per year)[32]. In contrast, the nine AAV-treated dogs with hemophilia A had a total of seven bleeding episodes during the combined total of 60 years of follow-up after AAV administration. The ABR per AAV-treated dog with hemophilia A was between 0.00 and 0.45 with a mean of 0.13 ± 0.16, lower than that reported for people with hemophilia on prophylaxis (ABRs of 4.8–6.0 bleeds per patient per year)[32].

Clinical blood chemistries were obtained two to four times per year from AAV-treated dogs to monitor for adverse reactions. The alanine aminotransferase (ALT) level was within the normal limits for six of the nine dogs at most of the time points analyzed (Fig. 2a,b). Woodstock and Linus had an elevation (<2 times the upper limit of normal) in ALT levels that began 4 years after AAV administration. These dogs were older (4 years old) at the time of vector administration than the other dogs studied. L51 also had ALT levels that were >2 times the normal limit at multiple time points and are considered mildly elevated[33]. The aspartate aminotransferase (AST) levels were within normal limits for all dogs for the duration of the study (Fig. 2c,d). These mild, asymptomatic elevations of liver enzyme levels were not consistent with a specific liver disease pattern. The serum α-fetoprotein (AFP) is a biomarker for hepatic disease, including HCC in some patients[34–36]. The AFP values for all dogs were within the normal range at all times analyzed (Fig. 2e,f). Other blood chemistries were monitored throughout the study without cause for clinical concern.

The liver pathology was evaluated at the final time point in the AAV-treated dogs with hemophilia A and compared to naive (to gene therapy) dogs with hemophilia A ($n=10$) or hemophilia B ($n=9$) and normal dogs ($n=9$) of similar age from the same colony (Supplementary Tables 1 and 2). Some of the findings were consistent with features commonly observed in older dogs and were seen in both AAV-treated and untreated (that is, naive) dogs. No pathologies definitively related to the treatment were identified. Three of nine AAV-treated dogs with hemophilia A had clinical symptoms that led to ending the study early, but none were believed to be related to AAV gene therapy (Methods).

The immune response to cFVIII (Supplementary Fig. 3) and neutralizing antibodies (NAbs) to the AAV capsid (Supplementary Table 3) were also followed during the study.

Investigation of the increase in FVIII expression. We investigated the mechanism of the increase in FVIII expression levels in Linus and M50 (Supplementary Table 4). At 6 years after vector administration, an ultrasound and liver biopsy were performed on Linus; no tumors, nodules or notable inflammation in the liver were detected. The increase in FVIII levels was not associated with changes in levels of circulating AFP, fibrinogen or von Willebrand factor (vWF) or clearance receptor in the liver (Fig. 2e,f and Supplementary Fig. 4).

We next assessed AAV vector copy number (VCN) (Table 1). For dogs that had multiple liver samples per lobe available for analysis, the VCNs showed that the vector was distributed throughout the liver (Supplementary Table 5). Higher VCN levels were not detected in Linus or M50. J60 had a higher VCN than the other dogs; we speculate that the splenectomy at the time of vector administration may have increased liver transduction.

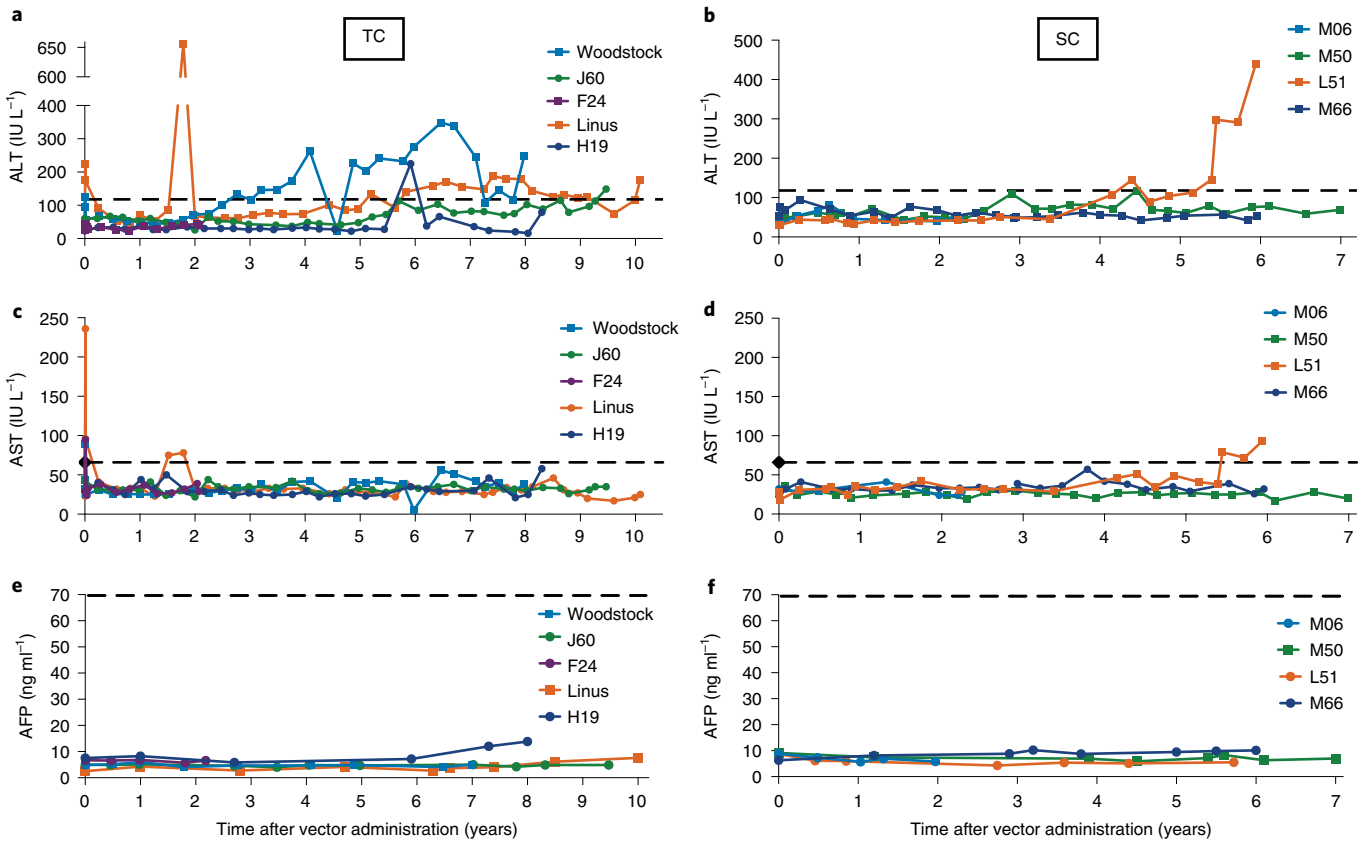

Fig. 2 | Assessment of liver function after AAV-cFVIII administration. ALT (**a**,**b**), AST (**c**,**d**) and AFP (**e**,**f**) levels were monitored after AAV administration and throughout the study. In each case, the *x* axis shows time in years and the *y* axis shows the liver analyte measured in blood. **a**,**c**,**e**, Dogs treated using the TC strategy. **b**,**d**,**f**, Dogs treated using the SC strategy. The upper limits of normal for ALT (120 IU L^{-1}), AST (65 IU L^{-1}) and AFP (70 ng ml^{-1}) are shown as dashed lines. Clinically, increases in liver enzyme levels in dogs are defined by veterinary clinical pathologists as mild (<5 times the upper limit of normal), moderate (5–10 times the upper limit of normal) or marked (>10 times the upper limit of normal)[33].

The pattern of cFVIII expression in the liver after AAV delivery was assessed by immunohistochemistry. Most of the tissue analyzed had cFVIII expression that was dispersed throughout the tissue, although some areas of the liver had what appeared to be clonal populations of cells expressing cFVIII (Extended Data Fig. 1). No major differences were noted between the dogs.

Analysis of integration site distributions in the livers of AAV-treated dogs. AAV vector genomes are expected to be present in multiple forms, with some integrated into the canine genome and some persisting as episomes. As integration can influence gene function and cell growth, we analyzed the locations of vector integration sites in the dog genome and the behavior of cell clones that harbored these integration sites.

We analyzed 20 samples of liver tissue taken at necropsy from six AAV-treated dogs and two untreated dogs with hemophilia A as controls. Liver DNA samples were selected to represent high, medium and low VCN ranges. Integration sites were recovered from genomic DNA samples by shearing DNA with sonication, ligating DNA linkers to the broken DNA ends, then carrying out nested PCR amplification using primers that bound to the ligated linker and the vector ITR sequences. (Supplementary Fig. 5). The resulting DNA fragments containing junctions between dog genomic DNA and vector DNA were then sequenced with the Illumina platform, and reads were mapped to the dog genome (CanFam3).

From these data, we can also estimate the clonal abundance of cells harboring each unique integrated vector. For a tissue sample containing DNA with expanded clones, there are be multiple DNA chains from each expanded clone that contain an identical integration site. Each chain is usually broken by sonication at a different location in the flanking dog DNA. As a result, there are different locations of adaptor ligation in the cellular DNA flanking the integration site. These points of adaptor ligation can then be quantified by sequencing from both ends of amplification products, providing a measure of the number of cells sampled[37].

We identified a total of 1,741 putative unique integration sites, corresponding to an inference of 3,263 sampled cells (Supplementary Table 6). Statistical analysis revealed modest but significant homology between AAV and canine sequences at vector–host junctions (Supplementary Fig. 6), suggesting that annealing of complementary DNA sequences promoted integration in at least some cases. The number of cells sampled per integration site ranged from 1 to 130; the high values indicate extensive clonal proliferation following the integration event. These expanded clones were scarce; unique integration sites recovered from at least three cells corresponded to only 4.8% of the cell population. No integration events were identified in the *Rian–Dlk–Dio* region (identified as canine chromosome 8, ~68,900,000–69,800,000), previously associated with AAV integration and transformation in mice[14,25]. The number of integration sites recovered per sample was positively correlated with VCN (Fig. 3a; $P = 3.0 \times 10^{-4}$). Most ITRs that were associated with integration were truncated (Supplementary Fig. 7), as seen in previous studies[13,38].

We selected 18 integration sites for validation by targeted PCR and Sanger sequencing, focusing on expanded clones. We succeeded

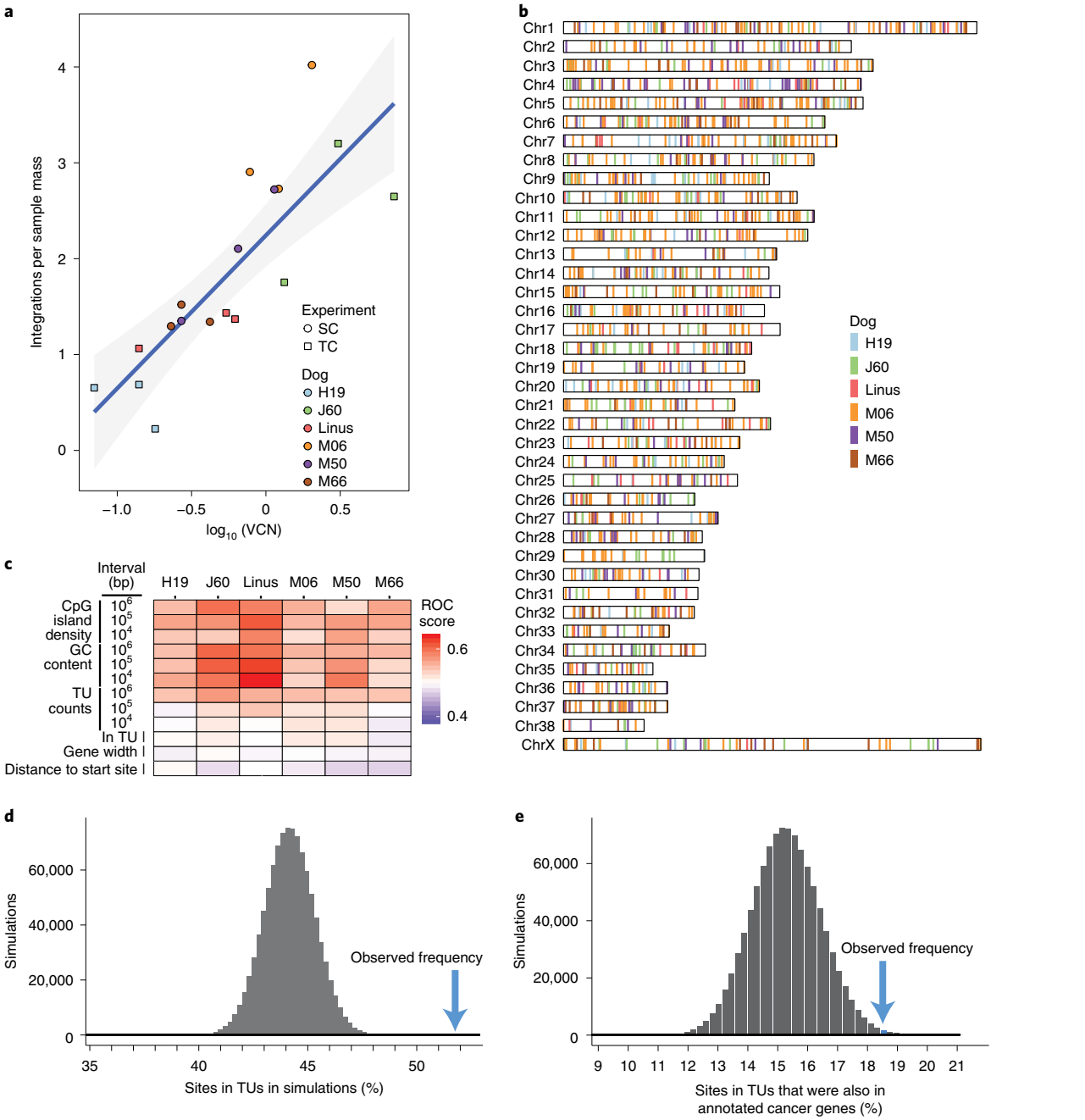

Fig. 3 | Distributions of AAV vector integration sites in the treated dogs. a, Correlation of the VCN value and the number of integration sites recovered from dog liver DNA specimens. Liver DNA samples ($n=3$ biologically independent samples) analyzed for each dog are shown as individual points. The gray envelope shows a 95% confidence interval. **b**, Distribution of AAV vector integration sites in the dog chromosomes. Chr, chromosome. **c**, Distribution of AAV vector integration sites in the dog genome relative to genomic annotation. Associations were calculated using the receiver operating characteristic (ROC) area method[30]. Values of the ROC area vary from 0 (negatively associated, blue) to 1 (positively associated, red). Several lengths of chromosomal intervals were used for comparison. **d**, Enrichment of integration sites in dog transcription units (TUs). The dark bars show the frequency of appearance of randomly selected sites in TUs, summarized over 10^6 random simulations. The blue arrow shows the observed frequency of AAV vector integration sites in TUs. **e**, Enrichment of integration sites within dog TUs that are also cancer-associated genes. A list of human cancer-associated genes[49] was used to annotate the dog genome.

in validating 13 sites (Supplementary Fig. 5 and Supplementary Table 7). Two sites that were found in negative controls could not be validated, indicating probable laboratory contamination.

Global analysis of integration site distributions showed that integration events were distributed throughout the dog chromosomes (Fig. 3b). Integration was significantly favored in transcription units (TUs) (Fig. 3c,d) and near CpG islands, which are associated with active transcription (Fig. 3c).

One possible contributor to cell persistence is insertional mutagenesis of genes involved in growth control. Comparison of our results to catalogs of cancer-associated genes in humans, mapped to canine homologs, showed that integration events were found

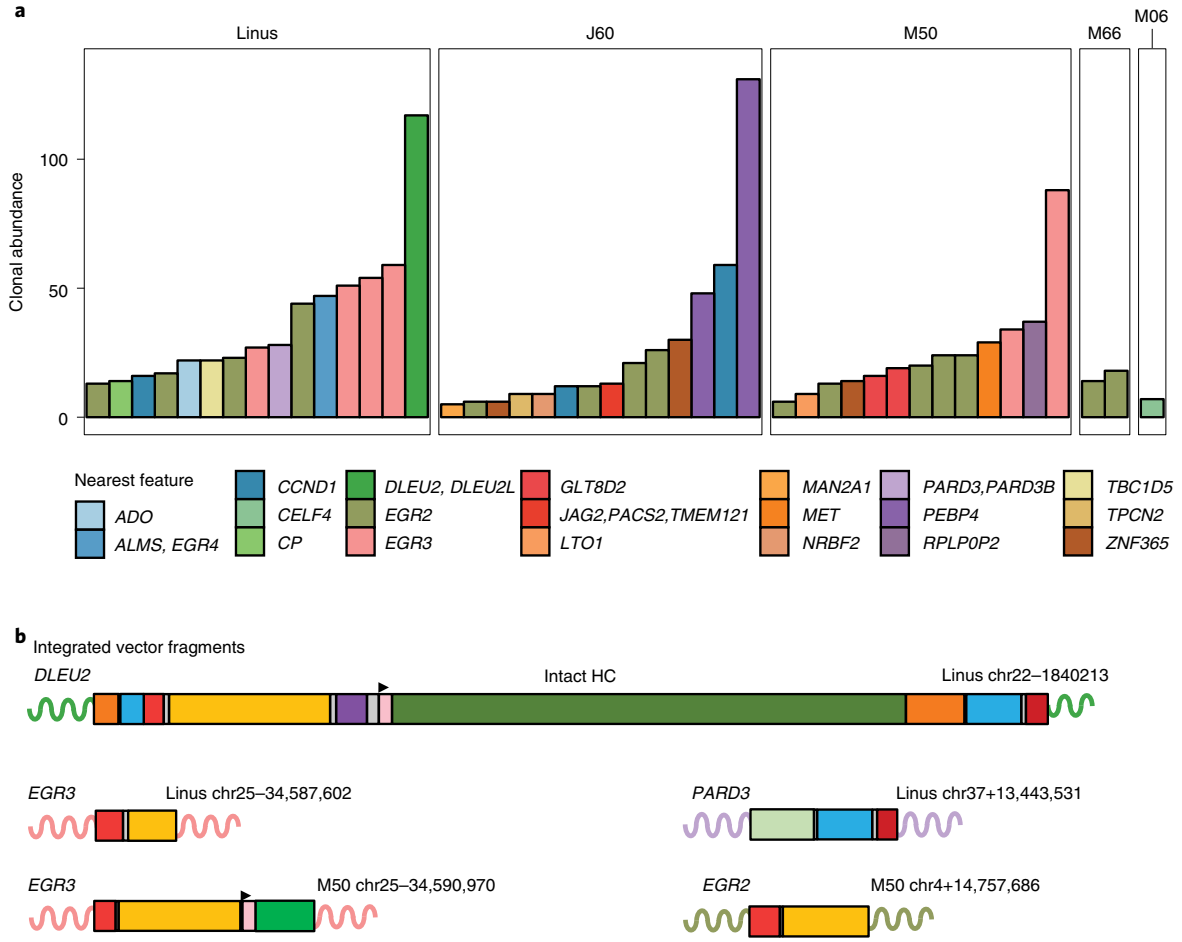

Fig. 4 | Clonal expansion of cells harboring AAV vectors. a, Summary of notable expanded clones in five of the six dogs studied. No expanded clones were detected in H19. Shown are the most abundant 15 clones per dog represented by five or more cells sampled. The genes affected are indicated by the color code. Data for each integration site studied are presented in Supplementary Table 12. **b**, Genetic map of vector sequences integrated in several of the dogs. The color code for vector segments is the same as in Fig. 1a. The schematics illustrate truncations and rearrangements that may not contain the entire vector sequence. Sequences are provided (NIH SRA BioProject ID: PRJNA606282). The numbers indicate the chromosome location and coordinates of a junction between AAV vector sequences and the dog genome. The gene at the site of integration is labeled. The curved lines represent genomic DNA at the site of integration, with the color matching the gene in **a**.

modestly more frequently in cancer-associated genes than expected by chance (Fig. 3e), and gene ontology analysis disclosed modestly higher integration frequency in genes from several pathways regulating cellular growth (Supplementary Table 9).

To assess possible effects of insertional mutagenesis on cellular proliferation, we studied the vector integration sites in the most expanded clones. The most expanded clones (≥5 cells; $n = 54$) are shown in Fig. 4a; all clones detected at least twice are in Supplementary Table 12. One challenge is that vector integration may mark a cell clone that expanded for a reason independent of insertional mutagenesis. Therefore, we looked for integrations that occurred multiple times independently in expanded clones from any of the dogs. Five genes were found at integration sites that expanded in multiple dogs (Fig. 4a): *EGR2* (four dogs), *EGR3* (two dogs), *CCND1* (two dogs), *LTO1* (two dogs) and *ZNF365* (two dogs). All these genes have been associated with transformation in humans. Two clones expanded beyond 100 cells, with vectors integrated at the genes 'deleted in leukemia 2' (*DLEU2*) and 'phosphatidylethanolamine binding protein 4' (*PEBP4*). In humans, *DLEU2* is a commonly deleted gene in leukemia[39]. The product of *PEBP4* is implicated as a modulator of signaling pathways in multiple cancer cell types[40,41].

Clustering of integration sites in the canine genome. Vector integration sites recovered in treated dogs can cluster on the target genome if integration at specific locations leads to increased cell growth or survival, so that at later times, cells with such integration events are present at increased frequency. We used model-independent scan statistics[42] to assess possible clustering and identified five clusters (limiting cluster sizes to less than 0.5 Mb). These corresponded to apparent clusters at *EGR2*, *EGR3*, *CCND1*, *ALB* and *DUSP1* (Supplementary Table 10). Genetic maps of clusters at *EGR2*, *EGR3* and *CCND1* are shown in Fig. 5. All three of these genes also hosted integration events in expanded clones, providing two different indications that integration at these genes was associated with preferential cell proliferation or persistence.

Structures of integrated vector DNA. As the structures of AAV vector sequences in cells can be complex[12,16,26], we investigated the structures of integrated vectors in expanded clones. We designed PCR primers that bound to the dog genome on either side of seven loci in expanded clones that were inferred to contain integrated vectors, amplified the full vector sequence and sequenced them by Illumina sequencing, successfully validating five loci (Fig. 4b and Supplementary Fig. 5).

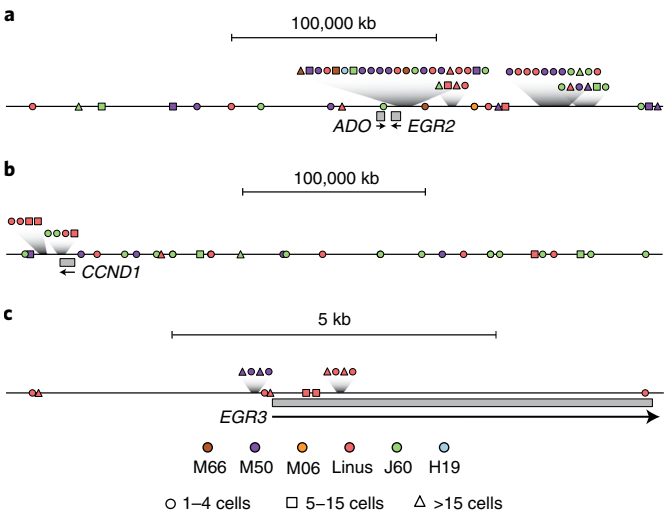

Fig. 5 | Three examples of clusters of AAV vector integration sites found in the dog genome. Clusters are shown schematically at *ADO–EGR2* (**a**), *CCND1* (**b**) and *EGR3* (**c**). TUs are indicated by gray rectangles. Integration sites are indicated by the shapes, with the inferred number of recovered cells harboring each site indicated by the nature of the shape (circle, 1–4 cells; square, 5–15 cells; and triangle, >15 cells). The colors of the shapes indicate the dog of origin. The scales are shown by the bar at the top.

The most expanded clone from Linus (integrated at *DLEU2*) contained an intact copy of the promoter and HC portion of the *F8* transgene (Fig. 4b). The ITRs were truncated at both ends, and in addition, a portion of the polyadenylation (polyA) site was duplicated. After extensive attempts, four additional integrants were also characterized, integrated in two cases at *EGR3* and one each at *PARD3* and *EGR2*. In all cases, the vectors were greatly truncated, resulting in transgene deletion and significant shortening of ITRs. Our reconstruction studies showed that intact ITRs inhibit PCR amplification, and internal repeat structures and longer concatemers were likely also recovered inefficiently, all of which could potentially bias the types of products recovered.

Rearrangements of the AAV vector. Our data provided additional evidence of extensive vector rearrangement. An average of 82% of integration sites showed apparent integration of AAV into *F8* itself (Supplementary Figs. 5 and 8). These could be confidently ascribed to vector rearrangements (that is, the apparent integration of the vector into itself) and not to integration into the genomic *F8* copy, based on three observations. 1) No integration was seen in introns of the cellular *F8* locus; introns were absent in the *F8* cDNA in the vector (Supplementary Figs. 9 and 10). 2) The B domain coding region of *F8*, which is absent in the vector but not in the genomic locus, lacked apparent integration sites (Supplementary Fig. 10). 3) Numerous sequence reads were seen in which the *F8* sequence crossed exon boundaries; such junctions were present in the *F8* cDNA but not the genomic locus (Supplementary Fig. 9). This documents the extensive formation of rearranged concatemeric AAV vector forms, which persisted in the dog liver for the full duration of the study. For most of the concatemers, it is not known whether they were integrated or episomal or whether the rearrangements occurred during vector production or in the target cells. Examples of rearranged sequences are shown in Supplementary Fig. 11. A previous report also identified the fusion of AAV vector sequences with each other as a prominent output from integration site analysis[43]

Discussion

After years of preclinical studies, AAV gene therapy for hemophilia A has yielded therapeutic levels of FVIII in human patients. Although the durability and safety of the approach remain mostly unstudied in humans, long-term outcomes can be readily evaluated in dogs. We have demonstrated that expression of FVIII can persist in dogs for as long as 10 years. Unexpectedly, two of the nine treated dogs had gradual increases in FVIII expression, reaching levels that were four-fold higher than those observed in the first 4 years. There were no clinical adverse events or evidence of malignancy related to AAV administration in any dog. Analysis of integration site distributions showed the expansion of clones that harbored vectors integrated in genes potentially associated with growth control.

The clinical phenotype correlated with the levels of FVIII expression. After AAV administration, there was a >97% reduction in the ABR (mean = 0.13 bleeds per year), even in dogs that expressed very low levels of FVIII. An ABR of <1 is lower than that reported for human patients on prophylaxis[32]. Because gene therapy provides continuous expression of FVIII, it has the advantage that the outcome does not depend on the maintenance of trough FVIII levels and compliance to a treatment regimen. Our data confirm that even low levels of FVIII achieved by gene therapy substantially improve the disease phenotype.

We considered several hypotheses that might explain the increase in FVIII expression in two of the dogs. The increase was independent of the delivery approach (TC versus SC), vector dose and promoter element (Supplementary Table 4). The TC and SC vectors had different promoter elements, *TBG* and *hAAT*, respectively. The *TBG* promoter has been linked to HCC in mouse models[14,28] while no studies have associated the *hAAT* promoter with HCC[12,14,44]. Both promoters are in clinical development (NCT03173521)[4,8]. The increase in FVIII expression levels was also not associated with any pathological findings, such as inflammation or biomarkers of hepatic disease.

The most plausible explanation emerged from the analysis of clonal behavior based on integration site analysis. Integration was favored in TUs, and, of the most expanded clones, 44% were found near genes that are associated with cell growth control and cancer in humans. However, we could document only one intact transgene in our sequence data (an intact HC at the *DLEU2* site in Linus), suggesting a potential role for unsampled expanded clones elsewhere in the liver to increase FVIII levels.

In previous studies, a 46-nucleotide liver-specific enhancer–promoter element adjacent to the wild-type AAV2 ITR was associated with cancer in humans[20–22]. In our integration site analysis, we used the 46-nucleotide element as the primer-binding site for our AAV primer by chance; therefore, this sequence was inferred to be present in all the AAV sequences reported here. The 46-nucleotide region is present in early AAV vectors[45] but not in many of the current clinical AAV vectors[22].

Structures of AAV sequences in dog livers were complex. Mapping of AAV sequences at five integration sites yielded only one vector with an intact transgene, and even that vector was truncated and partially rearranged. Rearrangements were identified in both TC- and SC-treated dogs, indicating that the large size of the transgene in the SC construct did not make it more prone to rearrangements. Fusion of vector ITRs to internal vector sequences was seen in 82% of all apparent integration sites. These events were clearly integrations into *F8* in the vector and not into the genomic *F8* locus, because numerous reads spanned exon boundaries, the B domain (deleted in the vector) was not targeted and no integration events were detected in *F8* introns. One implication of these data is that the VCN as usually measured in patient samples may greatly overestimate the number of functional copies of the encoded therapeutic gene. It will be of interest to investigate whether modification of the vector structure or the transduction procedure can increase

the proportion of intact transgenes ultimately present in target cells. Another question for future investigation is whether the structure of loci containing vector DNA changes over time after AAV infusion, for example, through iterative recombination that yields the greatly truncated vector derivatives observed at some integration sites (Fig. 4b).

This study has several limitations. The sample size is small, as is common in gene therapy studies of large vertebrates. Integration site analysis recovers some but not all integration events; therefore, inferences are based on incomplete data. Because of the sampling scheme used, we were unable to pair integration site analysis with an analysis of the expression of nearby host genes. In the integration site analysis, integration events associated with large deletions of the host chromosome could have been misidentified as two independent integration events. For the vector-into-vector integration events, it is unknown whether the sequences were integrated or episomal. Reconstruction studies showed that the DNA folding in the full ITR sequence interferes with efficient PCR, creating a possible recovery bias in favor of molecules with deleted ITRs. Lastly, hepatocytes can become polyploid during normal liver homeostasis, which could have been scored in our assays as low-level clonal expansion[46].

Our findings pose questions for ongoing gene therapy trials for hemophilia and other AAV gene therapy studies. To our knowledge, no previous study has documented an increase in FVIII expression levels after AAV-FVIII gene therapy in small or large animals. The FVIII levels in the dogs we studied remained within the range of a mild human hemophilia A phenotype; however, supraphysiological FVIII levels have been associated with thrombosis and would be concerning[47,48]. Although AAV clinical studies for hemophilia A, with 3 years of follow-up[4], and for hemophilia B, with about 10 years of follow-up[10], have not reported increases in transgene expression or vector-mediated serious adverse events, our data emphasize the importance of long-term monitoring after AAV gene therapy.

Online content

Any methods, additional references, Nature Research reporting summaries, source data, extended data, supplementary information, acknowledgements, peer review information; details of author contributions and competing interests; and statements of data and code availability are available at https://doi.org/10.1038/s41587-020-0741-7.

Received: 13 February 2020; Accepted: 15 October 2020;
Published online: 16 November 2020

References

1. Rangarajan, S. et al. AAV5-factor VIII gene transfer in severe hemophilia A. *N. Engl. J. Med.* **377**, 2519–2530 (2017).
2. High, K. A. et al. A phase 1/2 trial of investigational Spk-8011 in hemophilia A demonstrates durable expression and prevention of bleeds. *Blood* **132**, 487 (2018).
3. Nathwani, A. C. et al. GO-8: preliminary results of a phase I/II dose escalation trial of gene therapy for haemophilia A using a novel human factor VIII variant. *Blood* **132**, 489 (2018).
4. Pasi, K. J. et al. Multiyear follow-up of AAV5-hFVIII-SQ gene therapy for hemophilia A. *N. Engl. J. Med.* **382**, 29–40 (2020).
5. Jiang, H. et al. Multiyear therapeutic benefit of AAV serotypes 2, 6, and 8 delivering factor VIII to hemophilia A mice and dogs. *Blood* **108**, 107–115 (2006).
6. Sabatino, D. E. et al. Efficacy and safety of long-term prophylaxis in severe hemophilia A dogs following liver gene therapy using AAV vectors. *Mol. Ther.* **19**, 442–449 (2011).
7. Sarkar, R. et al. Long-term efficacy of adeno-associated virus serotypes 8 and 9 in hemophilia A dogs and mice. *Hum. Gene Ther.* **17**, 427–439 (2006).
8. Nathwani, A. C. et al. Long-term safety and efficacy of factor IX gene therapy in hemophilia B. *N. Engl. J. Med.* **371**, 1994–2004 (2014).
9. Nathwani, A. C. et al. Adeno-associated mediated gene transfer for hemophilia B: 8 year follow up and impact of removing 'empty viral particles' on safety and efficacy gene transfer. *Blood* **132**, 491 (2018).
10. Nakai, H. et al. Extrachromosomal recombinant adeno-associated virus vector genomes are primarily responsible for stable liver transduction in vivo. *J. Virol.* **75**, 6969–6976 (2001).
11. Schotanus, B. A., Penning, L. C. & Spee, B. Potential of regenerative medicine techniques in canine hepatology. *Vet. Q.* **33**, 207–216 (2013).
12. Li, H. et al. Assessing the potential for AAV vector genotoxicity in a murine model. *Blood* **117**, 3311–3319 (2011).
13. Nakai, H. et al. Large-scale molecular characterization of adeno-associated virus vector integration in mouse liver. *J. Virol.* **79**, 3606–3614 (2005).
14. Chandler, R. J. et al. Vector design influences hepatic genotoxicity after adeno-associated virus gene therapy. *J. Clin. Invest.* **125**, 870–880 (2015).
15. Chandler, R. J., Sands, M. S. & Venditti, C. P. Recombinant adeno-associated viral integration and genotoxicity: insights from animal models. *Hum. Gene Ther.* **28**, 314–322 (2017).
16. Zhong, L. et al. Recombinant adeno-associated virus integration sites in murine liver after ornithine transcarbamylase gene correction. *Hum. Gene Ther.* **24**, 520–525 (2013).
17. Gil-Farina, I. et al. Recombinant AAV integration is not associated with hepatic genotoxicity in nonhuman primates and patients. *Mol. Ther.* **24**, 1100–1105 (2016).
18. Kaeppel, C. et al. A largely random AAV integration profile after LPLD gene therapy. *Nat. Med.* **19**, 889–891 (2013).
19. Nault, J.-C. et al. Recurrent AAV2-related insertional mutagenesis in human hepatocellular carcinomas. *Nat. Genet.* **47**, 1187–1193 (2015).
20. La Bella, T. et al. Adeno-associated virus in the liver: natural history and consequences in tumour development. *Gut* **69**, 737–747 (2020).
21. Büning, H. & Schmidt, M. Adeno-associated vector toxicity—to be or not to be? *Mol. Ther.* **23**, 1673–1675 (2015).
22. Logan, G. J. et al. Identification of liver-specific enhancer-promoter activity in the 3′ untranslated region of the wild-type AAV2 genome. *Nat. Genet.* **49**, 1267–1273 (2017).
23. Bell, P. et al. No evidence for tumorigenesis of AAV vectors in a large-scale study in mice. *Mol. Ther.* **12**, 299–306 (2005).
24. Donsante, A. et al. Observed incidence of tumorigenesis in long-term rodent studies of rAAV vectors. *Gene Ther.* **8**, 1343–1346 (2001).
25. Donsante, A. et al. AAV vector integration sites in mouse hepatocellular carcinoma. *Science* **317**, 477 (2007).
26. Walia, J. S. et al. Long-term correction of Sandhoff disease following intravenous delivery of rAAV9 to mouse neonates. *Mol. Ther.* **23**, 414–422 (2016).
27. Rosas, L. E. et al. Patterns of scAAV vector insertion associated with oncogenic events in a mouse model for genotoxicity. *Mol. Ther.* **20**, 2098–2110 (2012).
28. Bell, P. et al. Analysis of tumors arising in male B6C3F1 mice with and without AAV vector delivery to liver. *Mol. Ther.* **14**, 34–44 (2006).
29. Lozier, J. N. et al. The Chapel hill hemophilia A dog colony exhibits a factor VIII gene inversion. *Proc. Natl Acad. Sci. USA* **99**, 12991–12996 (2002).
30. Sabatino, D. E. et al. Recombinant canine B-domain-deleted FVIII exhibits high specific activity and is safe in the canine hemophilia A model. *Blood* **114**, 4562–4565 (2009).
31. McCormack, W. M. et al. Helper-dependent adenoviral gene therapy mediates long-term correction of the clotting defect in the canine hemophilia A model. *J. Thromb. Haemost.* **4**, 1218–1225 (2006).
32. Berntorp, E., Spotts, G., Patrone, L. & Ewenstein, B. M. Advancing personalized care in hemophilia A: ten years' experience with an advanced category antihemophilic factor prepared using a plasma/albumin-free method. *Biologics* **8**, 115–127 (2014).
33. Center, S. A. Interpretation of liver enzymes. *Vet. Clin. North Am. Small Anim. Pract.* **37**, 297–333 (2007).
34. Galle, P. R. et al. Biology and significance of α-fetoprotein in hepatocellular carcinoma. *Liver Int.* **39**, 2214–2229 (2019).
35. Kitao, S. et al. α-fetoprotein in serum and tumor tissues in dogs with hepatocellular carcinoma. *J. Vet. Diagn. Invest.* **18**, 291–295 (2006).
36. Yamada, T. et al. Serum α-fetoprotein values in dogs with various hepatic diseases. *J. Vet. Med. Sci.* **61**, 657–659 (1999).
37. Berry, C. C. et al. Estimating abundances of retroviral insertion sites from DNA fragment length data. *Bioinformatics* **28**, 755–762 (2012).
38. Yang, C. C. et al. Cellular recombination pathways and viral terminal repeat hairpin structures are sufficient for adeno-associated virus integration in vivo and in vitro. *J. Virol.* **71**, 9231–9247 (1997).
39. Gaidano, G., Foà, R. & Dalla-Favera, R. Molecular pathogenesis of chronic lymphocytic leukemia. *J. Clin. Invest.* **122**, 3432–3438 (2012).
40. Huang, R. Q. et al. Knockdown of PEBP4 inhibits human glioma cell growth and invasive potential via ERK1/2 signaling pathway. *Mol. Carcinog.* **58**, 135–143 (2019).
41. Zhang, D. et al. PEBP4 promoted the growth and migration of cancer cells in pancreatic ductal adenocarcinoma. *Tumour Biol.* **37**, 1699–1705 (2016).
42. Berry, C. C., Ocwieja, K. E., Malani, N. & Bushman, F. D. Comparing DNA integration site clusters with scan statistics. *Bioinformatics* **30**, 1493–1500 (2014).

43. Cogné, B. et al. NGS library preparation may generate artifactual integration sites of AAV vectors. *Nat. Med.* **20**, 577–578 (2014).
44. Kao, C.-Y. et al. Incorporation of the factor IX Padua mutation into FIX-Triple improves clotting activity in vitro and in vivo. *Thromb. Haemost.* **110**, 244–256 (2013).
45. Samulski, R. J., Chang, L. S. & Shenk, T. A recombinant plasmid from which an infectious adeno-associated virus genome can be excised in vitro and its use to study viral replication. *J. Virol.* **61**, 3096–3101 (1987).
46. Donne, R., Saroul-Aïnama, M., Cordier, P., Celton-Morizur, S. & Desdouets, C. Polyploidy in liver development, homeostasis and disease. *Nat. Rev. Gastroenterol. Hepatol.* **17**, 391–405 (2020).
47. Kyrle, P. A. et al. High plasma levels of factor VIII and the risk of recurrent venous thromboembolism. *N. Engl. J. Med.* **343**, 457–462 (2000).
48. Rietveld, I. M. et al. High levels of coagulation factors and venous thrombosis risk: strongest association for factor VIII and von Willebrand factor. *J. Thromb. Haemost.* **17**, 99–109 (2019).
49. Sadelain, M., Papapetrou, E. P. & Bushman, F. D. Safe harbours for the integration of new DNA in the human genome. *Nat. Rev. Cancer* **12**, 51–58 (2011).

Methods

AAV administration in dogs with hemophilia A. Dogs with hemophilia A were maintained at the University of North Carolina, Chapel Hill. All procedures with the dogs were approved by the Institutional Animal Care and Use Committee at the University of North Carolina. Vector administration and cFVIII transgene constructs were previously described. The TC vector was delivered by the portal vein which requires exteriorization of the spleen[6,50]. While performing this procedure, one dog (J60) developed a small splenic laceration that bled despite attempts to close the wound with suture material. A decision was made to perform a splenectomy from which the dog recovered without sequelae. J60 had a decline in FVIII expression in the absence of any increase in levels of liver enzymes (Fig. 2a,c) or evidence of an immune response (Supplementary Fig. 3). The SC vector was delivered by intravenous infusion using a peripheral vein.

cFVIII activity, antigen and antibody assays. cFVIII activity was determined using the Chromogenix Coatest SP4 FVIII kit (DiaPharma) using normal canine plasma as a standard. Whole-blood clotting time assays were performed as previously described[6]. cFVIII antigen levels were determined by ELISA as previously described[6]. To confirm the observation that cFVIII activity and antigen levels increased over time in Linus and M50, the activity and antigen levels were each measured in a single assay. Anti-cFVIII antibodies were detected with cFVIII-specific IgG1 and IgG2 antibodies by ELISA[6]. In each IgG ELISA assay, the pretreatment baseline sample for each dog was used as a control and subtracted as the background for each dog for the duration of the study to account for any variation in the background for each assay. The Bethesda assay was used to measure anti-cFVIII NAbs as previously described[6].

Serological studies of antibody responses to the AAV vector. Heat-inactivated canine plasma samples were diluted (1:1 to 1:3,155) in heat-inactivated FBS before incubation with AAV8-chicken-β-actin-*Renilla* luciferase for 1 h at 37 °C. Plasma samples incubated with the AAV8 vector were transferred onto human embryonic kidney cells stably expressing Ad-E4 (ATCC, CRL-2784) and incubated overnight at 37 °C. Using the *Renilla* Luciferase Assay System (Promega) and a luminometer (Veritas Microplate Luminometer, Turner BioSystems), luciferase expression was assayed. The NAb titer was defined as the first dilution of the dog plasma at which there was 50% or greater inhibition of reporter gene expression compared to the untreated HA canine plasma control sample.

Annualized bleeding rate. Naive dogs with hemophilia A ($n=11$) from two litters were followed prospectively for 4 years to obtain a detailed bleeding history for the dogs. The AAV-treated dogs were monitored for bleeding events for the duration of the study. The ABR was calculated based on the total number of bleeding events per number of years on the study.

Quantitative PCR for DNA copy number analysis. DNA from liver samples from different liver lobes of treated dogs was isolated using the DNeasy Blood & Tissue kit (Qiagen). When multiple liver samples from each liver lobe were available, an analysis of the VCN per liver lobe was performed (Supplementary Table 5). Gene copy numbers from each sample were determined using real-time quantitative PCR (qPCR) with TaqMan (Thermo Fisher Scientific). Primers were designed to recognize either the *cF8* LC (forward, 5′-AAGTGGCACAGT TACCGAGGGAAT-3′; reverse, 5′-GCAACTGTTGAAGTCACAGCCCAA-3′; probe with a 5′ fluorescein derivative (6-FAM), Iowa Black FQ and Zen quenchers, 5′-AGTACATCCGTTTGCACCCAACCCAT-3′) or the *cF8* HC region (forward, 5′-AAGGGAGTCTGGCCAAAGAAAGGA-3′; reverse, 5′-CATTGATGGTGTG CAGCTCATGCT-3′; probe with a 5′ fluorescein derivative (6-FAM), Iowa Black FQ and Zen quenchers, 5′-AAATGCGTCTTTGACACAGGCTGAGG-3′). These primers bind within the *cF8* cDNA sequence, while the primers for the integration analysis bind outside of the *cF8* sequence (Analysis of AAV integration sites and Supplementary Table 11). The number of *cF8* copies was standardized against a series of dilutions of linearized pAAV plasmid containing the *cF8-BDD* (B domain deleted) transgene.

Assays to assess fibrinogen, AFP and vWF. Fibrinogen levels in plasma were assayed using the Canine Fibrinogen ELISA kit (ab205083, Abcam). Canine AFP was assayed in serum using a Dog AFP ELISA kit (Kamiya Biomedical). vWF was detected with an ELISA assay. Canine vWF in citrated plasma samples was captured using a rabbit anti-human vWF antibody (Dako, 95051) and detected using the same HRP-conjugated antibodies with the Lighting-Link HRP kit (Novus Biologicals).

Western blot analysis of LRP1. For western blot analysis of LRP1, whole-cell lysate extraction was carried out from frozen liver tissue using RIPA lysis buffer (Cell Signaling Technology) with a Complete Protease Inhibitor cocktail (Roche). Protein concentrations were determined using the Coomassie Bradford Protein Assay kit (Thermo Scientific), and similar amounts of proteins were loaded onto a NuPAGE 4–12% Bis-Tris gel (Thermo Fisher Scientific) under reducing conditions. Samples were then blotted onto a nitrocellulose membrane and detected using rabbit monoclonal anti-LRP1 antibodies (ab92544, Abcam) and goat anti-rabbit IgG (H&L) IRDye 800CW (925-32211, LI-COR). After LRP staining, the membrane was stripped using LI-COR Stripping Buffer (LI-COR) and stained for GAPDH as a loading control (mouse recombinant anti-GAPDH, 6C5, Abcam; goat anti-mouse IgG (H&L) IRDye 680RD, LI-COR). After densitometry, the levels of protein for each dog were adjusted based on GAPDH and normalized to those from an untreated dog with hemophilia A. An uncropped image of the western blot is provided in the Supplementary Data.

Immunohistochemistry. Liver samples were fixed in formalin before being embedded in paraffin. Slides (5 µm thick) were boiled in 1 mM EDTA for antigen retrieval in a microwave oven. Endogenous peroxidase was blocked using a 2.13% sodium meta-periodate buffer, followed by further blocking in buffer containing 5% goat serum (Cell Signaling Technology). FVIII was detected using a mouse monoclonal anti-cFVIII antibody or a rabbit polyclonal anti-cFVIII antibody (Green Mountain Antibodies), followed by a biotinylated goat anti-rabbit IgG antibody (Vector Laboratories). Slides were incubated with reagents from the VECTASTAIN ABC kit (Vector Laboratories), and immunohistochemical reactions were carried out using the SignalStain DAB Substrate kit (Cell Signaling Technology).

Analysis of anti-FVIII and anti-AAV antibodies. Although the dogs in this study had been exposed to plasma-derived cFVIII protein to treat bleeding episodes before vector delivery, they did not have any evidence of an immune response to cFVIII before AAV administration. Eight of the nine dogs had no evidence of anti-cFVIII antibodies throughout the study (Supplementary Fig. 2)[6].

NAbs to the AAV capsid can prevent the transduction of AAV at the time of vector administration or interfere with readministration. Before vector administration, the anti-AAV8 NAb titers were <1:1 in all dogs, except for one that showed possible low titers (1:1 to 1:3.16) (Supplementary Table 1). After AAV administration, titers rose to >1:3,000 and remained between 1:1,000 and 1:3,000 at the terminal time points. These data indicate that anti-AAV antibody titers persisted at high levels for years following AAV administration.

Liver pathology. The liver was removed within minutes after euthanasia in eight of the nine dogs. The one exception was Woodstock, who died from a fatal hemorrhage on the kidney. All five lobes were identified, palpated and examined for macroscopic abnormalities. All lobes were then cut into ~1-cm serial sections, and the cut surfaces were inspected for abnormalities. Samples were then taken from all five lobes that were snap-frozen in liquid nitrogen, frozen in optimal cutting temperature compound (Fisher Scientific) or placed in 10% buffered formaldehyde.

The liver histopathology was assessed by analysis of hematoxylin- and eosin-stained liver sections (Supplementary Tables 1 and 2). The veterinary pathologist who read these slides was blinded to the treatment groups. Two of the dogs had liver biopsies taken before AAV gene therapy (Woodstock and Linus), and one had a liver biopsy 6 years after gene therapy due to asymptomatic elevation of liver enzymes levels and then was followed for an additional 4 years (Linus). As a control for the potential effect of AAV gene therapy, liver sections from naive dogs with hemophilia A ($n=10$) or hemophilia B ($n=9$) and wild-type dogs ($n=9$) of similar age from the same colony were also analyzed. No definitive treatment-related findings were observed in any of the dogs examined. Most of the AAV-treated and control naive dogs in this study exhibited at least one of the following findings that were compatible with age-related or background changes seen in dogs. These changes included a slight increase in connective tissue within the portal regions and around central veins, mixed inflammatory cell infiltrates in the same regions, bile duct hyperplasia, variable numbers of inflammatory cell aggregates and lipogranulomas, subcapsular post-necrotic scars and multifocal nodular hyperplasia. In some cases, the connective tissue minimally extended away from the portal and centrilobular regions, without definitive evidence of bridging between these regions.

Acute hepatocellular necrosis was observed in one AAV-treated dog, H19, and mainly involved the centrilobular region. While an effect of the AAV treatment could not be entirely ruled out, it was considered less likely, given the distribution and time since the treatment administration (8.3 years). The history of severe diarrhea that required the euthanasia of this dog likely played a role in this phenomenon (that is, hypovolemia and/or endotoxin translocation from the gastrointestinal tract).

Although more commonly seen in association with hyperadrenocorticism (that is, Cushing's disease or exogenous steroid administration), the hepatocellular swelling and clearing seen in most dogs can likely be considered as a background finding. This change may be associated with cytoplasmic glycogen accumulation and osmotic fluid intake. Alternatively, prolonged fixation of the tissues in buffered 10% formaldehyde may have contributed to these changes, which would then be artifacts due to tissue processing. These findings are likely not consequential, given that levels of liver enzymes were not significantly elevated. Of the nine pathological variables assessed (Supplementary Tables 1 and 2), only hepatocellular swelling and clearing showed a significant difference between the AAV-treated and naive dogs with hemophilia A (exact Wilcoxon–Mann–Whitney test[51], $P=0.004$). However,

the AAV-treated dogs with hemophilia A were also significantly older than the naive dogs at time of necropsy (8.9 versus 5.5 years), and when the AAV-treated animals were compared to older naive wild-type dogs, there was no significant difference in hepatocellular swelling. Thus, further studies are needed to determine whether this pathology is associated with age or with treatment.

Of the three AAV-treated dogs with increased levels of ALT, Woodstock and Linus exhibited slightly more swelling and clearing than other dogs, while L51 did not have any evidence of hepatocyte swelling or clearing. The latter dog presented with more pronounced hemosiderin-laden macrophages, which likely represents sequelae to small hemorrhages. In contrast, dog M06 presented similar levels of hepatocyte swelling and clearing as Woodstock and Linus, without the associated increase in levels of liver enzymes. A definitive histopathologic explanation for the increased ALT levels in these three dogs was difficult to ascertain.

Liver stained with hematoxylin and eosin from naive (to gene therapy) dogs with hemophilia A or hemophilia B and wild-type dogs were also analyzed (Supplementary Table 2). These dogs were similar in age to the AAV-treated dogs with hemophilia A in this study. The mean age of the dogs at the time of necropsy was 5.5 ± 2.2 years for the dogs with hemophilia A, 5.6 ± 3.1 years for those with hemophilia B and 11.7 ± 2.4 years for the wild-type dogs. The changes seen in these naive dogs were very similar to the age-related changes seen in the AAV-treated dogs with hemophilia A, both in the type of lesion and degree of severity. Three naive control dogs had elevations in levels of their liver enzymes (alkaline phosphatase) (P19, X13, I32). The liver capsule in P19, a naive dog with hemophilia A, was regionally thickened and fibrotic and was elevated by a large accumulation of hemosiderin-laden macrophages and fibrous connective tissue. This likely represented a focus of chronic hemorrhage. Two additional naive dogs (G35, hemophilia B; Diamond, hemophilia A) showed vascular changes that may be related to either amyloid deposition or arteriosclerosis. Three naive dogs had malignant neoplasms in their liver. Based on the hematoxylin and eosin staining, the neoplasms were diagnosed as of epithelial origin (Elton, wild type), metastatic osteosarcoma (I34, wild type) and lymphoma (O94, hemophilia A).

Clinical reasons for early termination. While six of the dogs were followed until the end of the study without clinical concerns, three dogs had clinical issues that led to the termination of the study. H19 had severe diarrhea and weight loss for unknown reasons and was euthanized 8.3 years after AAV administration. M06 had recurring rectal bleeds due to mucosal polyps and was euthanized 2.3 years after vector administration. Woodstock was found deceased 8.8 years after AAV delivery and, upon autopsy, the cause of death was determined to be a hemorrhage on the kidney. None of these clinical observations were related to AAV administration.

Analysis of AAV integration sites. Six dogs were selected for AAV integration analysis, the two dogs that had an increase in FVIII expression, Linus (TC approach) and M50 (SC approach), and the dogs that received the same AAV dose of the TC vector (H19) or the SC vector (M06) were included as controls to analyze alongside Linus and M50. In addition, one of the high-dose TC-treated dogs and one of the low-dose SC-treated dogs were included for comparison (see Table 1). Integration site isolation and sequencing were carried out using ligation-mediated PCR[52] under the following conditions. DNA for each sample (60–250 ng) was sheared using a Covaris M220 ultrasonicator to achieve a fragment size of roughly 1,000 bp under the following conditions: peak power, 50 W; duty factor, 2%; cycles, 200 for 95 s. Two negative controls were added, for which molecular-grade water was used instead of DNA. Bead purification of sheared DNA and linker ligation were performed as previously described[52]. The first PCR reaction (PCR1) was performed in triplicate to suppress effects of PCR jackpotting, with a total volume of 25 µl per reaction, 300 nM PCR1 linker primer, 300 nM ITR primer 1, 1× Clontech Advantage 2 PCR Buffer (Takara Bio), 200 µM dNTPs and 1× Clontech Advantage 2 Polymerase Mix (Takara Bio). PCR1 thermocycling parameters were as follows: initial denaturation for 1 min at 95 °C, five linear amplification cycles of 95 °C for 30 s, 80 °C for 30 s (annealing) and 72 °C for 1 min 30 s (extension), followed by 20 exponential amplification cycles of 95 °C for 30 s, 80 °C for 30 s (annealing) and 70 °C 1 min 30 s (extension), followed by a final extension at 72 °C for 4 min and an infinite hold at 4 °C. Two microliters of PCR1 product were diluted into the second PCR reaction (PCR2), performed in triplicate, with a total volume of 25 µl per reaction, 300 nM PCR2 linker primer, 300 nM ITR primer 2, 1× Clontech Advantage 2 PCR Buffer (Takara Bio), 200 µM dNTPs and 1× Clontech Advantage 2 Polymerase Mix (Takara Bio). PCR2 thermocycling parameters were as follows: 1 min initial denaturation at 95 °C, five linear amplification cycles of 95 °C for 30 s, 80 °C for 30 s (annealing) and 72 °C for 1 min 30 s (extension), followed by 15 exponential amplification cycles of 95 °C for 30 s, 80 °C for 30 s (annealing), at 70 °C 1 min 30 s (extension), followed by a final extension at 72 °C for 4 min and an infinite hold at 4 °C. Finally, samples were pooled, purified and quantified as previously described and sequenced on an Illumina MiSeq with a library loading concentration of 10 pM, and PhiX was spiked in at 15%.

Computational analysis of AAV integration sites. AAV integrations were identified with the AAVenger software pipeline, which identifies AAV integrations from paired-end sequencing data, in which sequenced fragments begin with the internal edge of integrated AAV ITR sequences and end with flanking genomic sequences. ITR sequence remnants were recorded, after which viral and adaptor sequences were removed from sequencing reads before alignment to the host genome with the BLAT aligner. Aligned reads were then assembled into genomic fragments in which the number of unique fragment lengths associated with integration positions was used as a lower-end estimate for clonal abundance[53].

The canine genome was annotated using a sequence homology xenoRef human annotation track (https://genome.ucsc.edu/cgibin/hgTrackUi?hgsid=866058135_C33ztc5VtUOsQYEJhmgFwr4Xh4sH&c=chr26&g=xenoRefGene). This track was produced at UCSC from RNA sequence data generated by scientists worldwide and curated by the NCBI RefSeq project[54,55]. The RNA sequences were aligned against the dog genome using BLAT[56]; those with an alignment of less than 15% were discarded. When a single RNA sequence aligned in multiple locations, the alignment having the highest base identity was used. Only alignments having a base identity level within 0.5% of the best and at least 25% base identity with the genomic sequence were retained.

The AAVenger software, raw sequencing data and analysis software supporting this study are available at the Zenodo data server (https://doi.org/10.5281/zenodo.3666122), while the demultiplexed sample reads that were generated during the analysis are available at the NIH SRA (BioProject ID: PRJNA606282).

Numbers of AAV integration site junctions expected to be present in assay reactions. Following recovery of integration sites using Illumina sequencing, we sought to validate several of the sites using targeted amplification and Sanger sequencing. As a first step, we calculated the expected numbers of target sequences in available samples. We approximated the number of integration site junctions from VCN and relative sonic abundance data as follows.

$$\frac{\text{Abundance of integration}}{\text{ng DNA}} = \frac{1,000 \text{ canine genomes}}{5.5 \text{ ng}} \times \frac{\text{AAV copies}}{\text{genome}} \times \frac{\text{abundance of integration}}{\text{AAV copy}}$$

One thousand canine genomes per 5.5 ng DNA is the size of the canine genome, AAV copies per genome is the VCN of the DNA sample, and abundance of integration per AAV copy is the relative sonic abundance of the integration site of interest (Supplementary Tables 7 and 8). For each AAV ITR-to-genomic PCR amplification, we maximized the number of integration site junctions in the PCR template input while never using more than 10% of the sample per PCR reaction (Supplementary Tables 7 and 8). For the long amplification of the high abundance integration into *DLEU2*, we input approximately 400 integration site junctions per PCR reaction, performing reactions in triplicate and using a total of 26% of the DNA sample.

Validation of AAV integration site data. In reconstruction experiments, we found that amplification across intact AAV ITR structures was inefficient, presumably due to extensive DNA secondary structure. In our sequence data, the great majority of ITRs were found to be truncated (Supplementary Fig 6). Based on previous literature[14,38], we suggest that these probably provide a representative sample of the authentic population of integrants, but it remains possible that the data were biased in favor of recovering integrants with truncated ITRs.

AAV integration results in heterogeneous junctions; therefore, it can be challenging to distinguish between authentic AAV integration events in the dog genome and artifactual molecules containing AAV and dog sequences generated during the PCR steps used to make sequence libraries. For this reason, we validated a set of the observed junctions using targeted PCR and Sanger sequencing.

Twenty integration sites were chosen for validation. These included high abundance sites in inferred expanded clones near cancer-associated genes, sites from less prominent clones and two sites from negative control dogs that were expected to be artifacts. Primers were chosen so that one matched the expected sequence of the AAV ITR near the AAV–dog DNA junction, and the second primer was chosen to match flanking dog DNA. Of the 18 sites from AAV-treated dogs, 13 could be validated by target PCR (Supplementary Tables 7 and 8). Neither of the two sites from negative controls could be validated (Supplementary Tables 7 and 8). Thus, we were successful in validating integration sites in expanded clones and partially successful in validating sites in rare clones.

Primer designs are shown in Supplementary Table 11. We designed forward and reverse genomic primers to flank each integration site and an additional primer to bind to both the 5′ and 3′ AAV ITR regions (Supplementary Table 11). Before amplifying samples from the livers of treated dogs, we verified that dog genomic primers flanking the expected integration site yielded dog genomic DNA products of the expected size, when tested in PCR reactions. We then performed 40 PCR reactions using the dog genomic forward primer or reverse primer paired with an AAV ITR primer binding to the A region of the ITR that is common to both ends of the genome. Dog liver DNA samples were amplified in a total volume of 25 µl with 2.5 U LongAmp *Taq* DNA Polymerase (New England Biolabs), 1× LongAmp *Taq* Reaction Buffer (New England Biolabs), 300 µM dNTPs, 0.4 µM forward primer and 0.4 µM reverse primer. PCR thermocycling parameters were as follows: 30 s initial denaturation at 94 °C, 35 cycles of 94 °C for 30 s, 60 °C for

30 s (annealing), at 65 °C for 30 s (extension), followed by an infinite hold at 4 °C. Each primer combination was also tested on negative control canine DNA in PCR reactions with the same chemical and thermocycling conditions to identify PCR products resulting from mispriming events.

PCR products were separated by electrophoresis on 1% agarose–TAE gels and visualized after staining with ethidium bromide. Substantial bands in experimental or negative canine control samples were cut from gels, and DNA was extracted from the bands with a Monarch DNA Gel Extraction Kit (New England Biolabs). The Concentration of extracted DNA was measured with a Quant-iT PicoGreen dsDNA Assay kit (Invitrogen). Extracted DNA was sequenced on a 3730xl sequencer (Applied Biosystems) in the Penn Genomics Analysis Core at the University of Pennsylvania. Fragments were sequenced from the genomic direction, or from the genomic and the AAV ITR directions when enough DNA product was available. Sequence results were tested for alignment to the canine genome using the BLAT search tool from the University of California, Santa Cruz. Results of validation attempts are summarized in Supplementary Table 7. Of 20 attempts at validation, 13 were successful. Two of the validation failures were apparent integration sites in untreated dogs, which we ascribed to laboratory contamination. Over all the integration site data and validation data, we identified both ends of 17 integrated AAV vectors (assuming that junctions with dog DNA were within 100 bp in the expected orientations). Failures were likely due to deletions in the vector, target site or both[15,24,25,38].

The high abundance integration at the *DLEU2* gene in Linus was further investigated by use of long-range PCR amplification. A complication is that reconstruction studies showed that amplification even from a plasmid template containing two full ITRs was undetectable. Conditions for this test were as follows: full-length FVIII AAV plasmid DNA was amplified with the two primer pairs designed to bind to the plasmid, 350 nucleotides or 2 kb away from the ITR fragments. In each reaction, 10 ng full-length FVIII AAV plasmid were amplified in a total volume of 25 µl with the following components: 2.5 U LongAmp *Taq* DNA Polymerase (New England Biolabs), 1× LongAmp *Taq* Reaction Buffer (New England Biolabs), 600 µM dNTPs, 0.4 µM forward primer and 0.4 µM reverse primer. PCR thermocycling parameters were as follows: 4 min initial denaturation at 94 °C, 40 cycles of 94 °C for 30 s, 60 °C for 1 min (annealing) and 65 °C for 41 min 40 s (extension), followed by a final extension at 65 °C for 10 min and an infinite hold at 4 °C. These conditions did not produce fragments of expected sizes. Further reconstruction studies under similar conditions showed that amplification could be accomplished through a single intact ITR. However, the *DLEU2* insertion event in Linus was associated with deleted ITRs; therefore, amplification was attempted across the full integration AAV vector at this locus. The forward and reverse dog genomic primers at position 1840213 in chromosome 22 were used to amplify the template DNA of interest in a PCR reaction with the following components: 2.5 U LongAmp *Taq* DNA Polymerase (New England Biolabs), 1× LongAmp *Taq* Reaction Buffer (New England Biolabs), 600 µM dNTPs, 0.4 µM forward primer and 0.4 µM reverse primer. PCR thermocycling parameters were as follows: initial denaturation at 94 °C for 30 s, 30 cycles of 94 °C for 30 s, 60 °C for 1 min (annealing) and 65 °C for 18 min 20 s (extension), followed by a final extension at 65 °C for 10 min and an infinite hold at 4 °C. Extension time was calculated from the polymerase's capacity to amplify 1 kb every 50 s, targeting a maximum amplification length of 22 kb.

PCR products were isolated after electrophoresis on a 1% agarose–TAE gel. Bands corresponding to a length of 4.9 kb were excised, and DNA was extracted from the bands with a Monarch DNA Gel Extraction kit (New England Biolabs). The concentration of extracted DNA was measured with a Quant-iT PicoGreen dsDNA Assay kit (Invitrogen).

Samples were prepared for metagenomic sequencing using the Nextera XT DNA Library Prep kit (Illumina), as per the manufacturer's guidelines. Samples were quantified by the Quant-iT PicoGreen dsDNA Assay kit and pooled based on concentration. The sequencing libraries were quantified by KAPA qPCR (Kapa Biosystems) and the Qubit dsDNA High-Sensitivity assay (Thermo Fisher Scientific), and fragment lengths were determined by TapeStation (Agilent). Libraries (8–10 pM) were sequenced on the Illumina MiSeq with dual-indexed barcodes and 2×250 bp read lengths.

Reporting Summary. Further information on research design is available in the Nature Research Reporting Summary linked to this article.

Data availability

The raw sequencing data supporting this study are available at the Zenodo data server (https://doi.org/10.5281/zenodo.3666122), while demultiplexed sample reads generated during the analysis are available at the NIH SRA (BioProject ID: PRJNA606282). Source data are provided with this paper.

Code availability

The AAVenger software and analysis software supporting this study are available at the Zenodo data server (https://doi.org/10.5281/zenodo.3666122). Source data are provided with this paper.

References

50. Sherman, A. et al. Portal vein delviery of viral vectors for gene therapy for hemophilia. *Methods Mol. Biol.* **1114**, 413–426 (2014).
51. Hothorn, T., Hornik, K., van de Wiel, M. & Zeileis, A. Implementing a class of permutation tests: the coin package. *J. Stat. Softw.* **28**, 1–23 (2008).
52. Sherman, E. et al. INSPIIRED: a pipeline for quantitative analysis of sites of new DNA integration in cellular genomes. *Mol. Ther. Methods Clin. Dev.* **4**, 39–49 (2017).
53. Berry, C. C. et al. INSPIIRED: quantification and visualization tools for analyzing integration site distributions. *Mol. Ther. Methods Clin. Dev.* **4**, 17–26 (2017).
54. Pruitt, K. D., Tatusova, T. & Maglott, D. R. NCBI Reference Sequence (RefSeq): a curated non-redundant sequence database of genomes, transcripts and proteins. *Nucleic Acids Res.* **33**, D501–D504 (2005).
55. Pruitt, K. D. et al. RefSeq: an update on mammalian reference sequences. *Nucleic Acids Res.* **42**, D756–D763 (2014).
56. Kent, W. J. BLAT—the BLAST-like alignment tool. *Genome Res.* **12**, 656–664 (2002).

Acknowledgements

We are grateful to members of the Sabatino and Bushman laboratories for help and suggestions. We acknowledge the Research Vector Core at the Children's Hospital of Philadelphia for production of the SC AAV vectors and the Penn Vector Core at the University of Pennsylvania for preparing the TC AAV vectors. We thank M. Keiser for assistance with immunohistochemistry and A. Messer for assisting with the analysis of the canine samples. We also thank N. Hoepp for discussions on canine liver clinical pathology. We thank S. Sherrill-Mix for help with statistical analysis. This work was supported by grants from the National Institutes of Health (RO1HL083017 (H.H.K.), R24HL63098 and N0175N92019D00041 (T.C.N.), RO1HL126850 (D.E.S.) and RO1AI082020, RO1CA241762, RO1HL142791 and U19AI149680 (F.D.B)). We also acknowledge support from the Penn Center for AIDS Research (P30AI045008) and the PennCHOP Microbiome Program (F.D.B.).

Author contributions

G.N.N., J.K.E., S.K., H.E.R., A.M.R., J.L. and C.W. performed the experiments. E.P.M., C.T.L. and T.C.N. performed the vector administration, sample collection and follow-up with the dogs. C.A.-A. performed the dog liver histopathology analysis. D.E.S., H.H.K., T.C.N. and F.D.B. designed the experiments. D.E.S. and F.D.B. wrote the manuscript.

Competing interests

D.E.S. receives royalties from a licensing agreement with Spark Therapeutics. D.E.S. and G.N.N. are inventors on a patent on FVIII and hemophilia A gene therapy.

Additional information

Extended data is available for this paper at https://doi.org/10.1038/s41587-020-0741-7.

Supplementary information is available for this paper at https://doi.org/10.1038/s41587-020-0741-7.

Correspondence and requests for materials should be addressed to D.E.S.

Reprints and permissions information is available at www.nature.com/reprints.

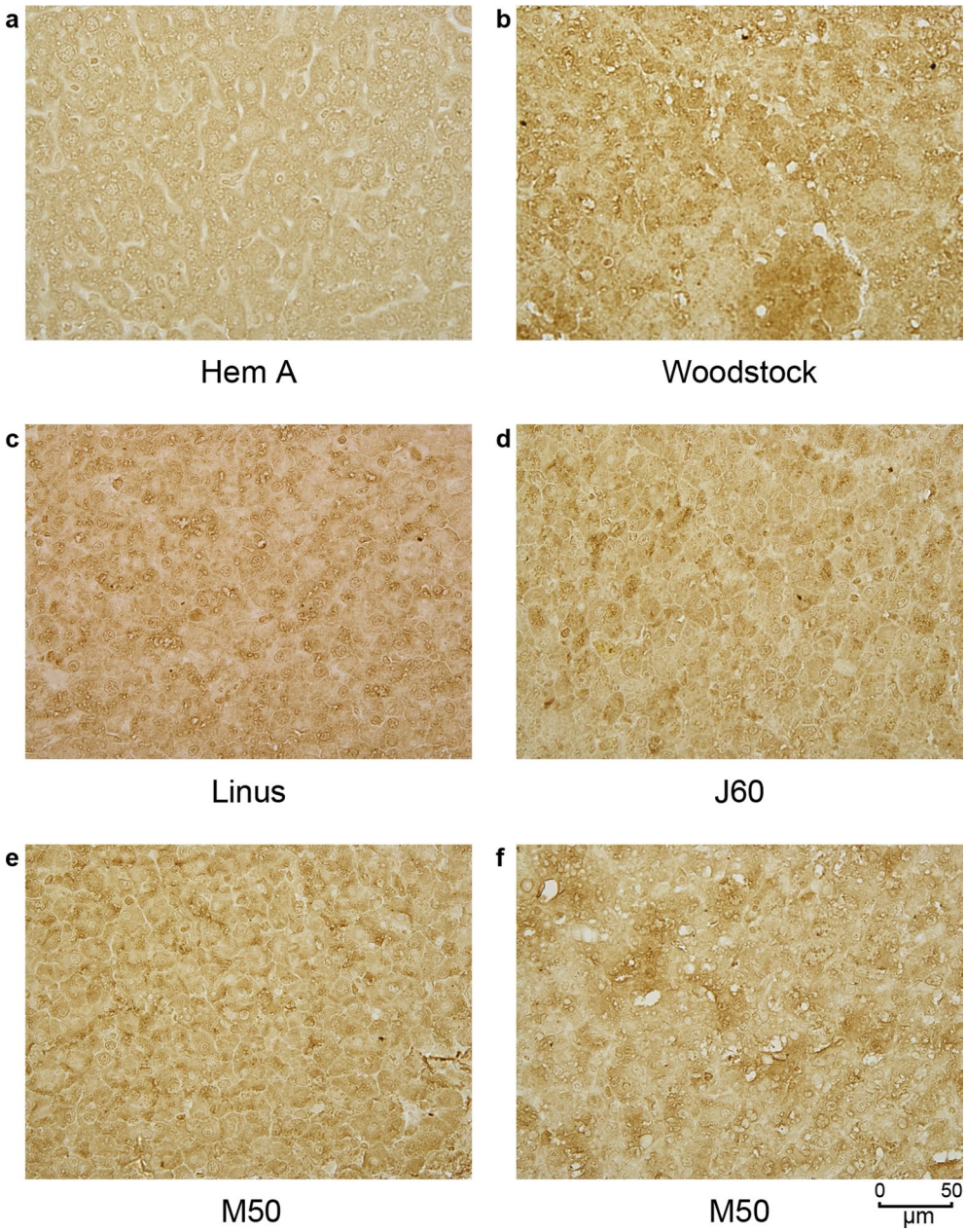

Extended Data Fig. 1 | Immunohistochemical detection of FVIII in liver after AAV administration. Immunohistochemical detection of FVIII in the liver from untreated (Hem A) (**a**) and treated (**b**,**c**,**d**,**e**,**f**) hemophilia A dogs. Locations of FVIII production are indicated by the brown stain. Most of the cFVIII staining was pan-lobular in distribution (b,c,d,e) while some areas had what appeared to be small clonal populations of cells that express cFVIII (**b,f**). Liver sections from multiple lobes were stained in n = 4 independent experiments. Images are representative of each dog. Scale bar representing 50μm applies to all images.

nature research

Corresponding author(s): Sabatino, Denise E.

Last updated by author(s): Oct 3, 2020

Reporting Summary

Nature Research wishes to improve the reproducibility of the work that we publish. This form provides structure for consistency and transparency in reporting. For further information on Nature Research policies, see Authors & Referees and the Editorial Policy Checklist.

Statistics

For all statistical analyses, confirm that the following items are present in the figure legend, table legend, main text, or Methods section.

n/a	Confirmed	
☐	☒	The exact sample size (*n*) for each experimental group/condition, given as a discrete number and unit of measurement
☐	☒	A statement on whether measurements were taken from distinct samples or whether the same sample was measured repeatedly
☐	☒	The statistical test(s) used AND whether they are one- or two-sided *Only common tests should be described solely by name; describe more complex techniques in the Methods section.*
☒	☐	A description of all covariates tested
☒	☐	A description of any assumptions or corrections, such as tests of normality and adjustment for multiple comparisons
☐	☒	A full description of the statistical parameters including central tendency (e.g. means) or other basic estimates (e.g. regression coefficient) AND variation (e.g. standard deviation) or associated estimates of uncertainty (e.g. confidence intervals)
☐	☒	For null hypothesis testing, the test statistic (e.g. *F*, *t*, *r*) with confidence intervals, effect sizes, degrees of freedom and *P* value noted *Give P values as exact values whenever suitable.*
☒	☐	For Bayesian analysis, information on the choice of priors and Markov chain Monte Carlo settings
☒	☐	For hierarchical and complex designs, identification of the appropriate level for tests and full reporting of outcomes
☒	☐	Estimates of effect sizes (e.g. Cohen's *d*, Pearson's *r*), indicating how they were calculated

Our web collection on statistics for biologists contains articles on many of the points above.

Software and code

Policy information about availability of computer code

Data collection	All sequencing reads used in this study are available from the NIH SRA (BioProject ID: PRJNA606282).
Data analysis	All analysis code and results supporting this study are available from the Zenodo data server (DOI 10.5281/zenodo.3666122)

For manuscripts utilizing custom algorithms or software that are central to the research but not yet described in published literature, software must be made available to editors/reviewers. We strongly encourage code deposition in a community repository (e.g. GitHub). See the Nature Research guidelines for submitting code & software for further information.

Data

Policy information about availability of data

All manuscripts must include a data availability statement. This statement should provide the following information, where applicable:

- Accession codes, unique identifiers, or web links for publicly available datasets
- A list of figures that have associated raw data
- A description of any restrictions on data availability

All software, raw sequencing data, and analysis software supporting this study is available at the Zenodo data server (DOI 10.5281/zenodo.3666122) while demultiplexed sample reads generated during the analysis are available at the NIH SRA (BioProject ID: PRJNA606282).

Field-specific reporting

Please select the one below that is the best fit for your research. If you are not sure, read the appropriate sections before making your selection.

☒ Life sciences ☐ Behavioural & social sciences ☐ Ecological, evolutionary & environmental sciences

Life sciences study design

All studies must disclose on these points even when the disclosure is negative.

Sample size	The samples size was determined based on previous studies of AAV delivery of a transgene in a large animal model. Five hemophilia A dogs were treated with the two-chain delivery approach and four dogs were treated with the single-chain delivery approach. Six of the dogs were utilized for the AAV integration studies. The numbers of biologically independent samples from these dogs are reported as applicable.
Data exclusions	No data was excluded from the analyses.
Replication	Assays were repeated at least two times and these replication attempts were successful. For the AAV integration studies, multiple independent liver samples (n=3 per dog) originating from different liver lobes from six canine subjects were sequenced in order to characterize integration events within each dog. Each liver lobe sample was sequenced once in order to maximize read depth and provide the broadest possible sampling of the integration events.
Randomization	Not relevant.
Blinding	The liver pathology analysis of the AAV-treated dogs and naive dogs was performed by the veterinary pathologist blinded to the dog and treatment.

Reporting for specific materials, systems and methods

We require information from authors about some types of materials, experimental systems and methods used in many studies. Here, indicate whether each material, system or method listed is relevant to your study. If you are not sure if a list item applies to your research, read the appropriate section before selecting a response.

Materials & experimental systems

n/a	Involved in the study
☐	☒ Antibodies
☐	☒ Eukaryotic cell lines
☒	☐ Palaeontology
☐	☒ Animals and other organisms
☒	☐ Human research participants
☒	☐ Clinical data

Methods

n/a	Involved in the study
☒	☐ ChIP-seq
☒	☐ Flow cytometry
☒	☐ MRI-based neuroimaging

Antibodies

Antibodies used	Rabbit Anti-human vWF (Dako A0082 polyclonal lot#: 20051016) at 1:500 dilution Anti-LRP1 antibodies (Abcam ab92544 monoclonal) at 1:50000 dilution Goat Anti-rabbit IgG (H+L) IRDye 800 CW (Li-Cor 925-32211 lot#: C80118-01) at 1:15000 Mouse recombinant Anti-GAPDH (Abcam 6C5) at 1:500 dilution Goat Anti-mouse IgG (H+L) IRDye 680RD (Li-COR 925-68070) at 1:15000 Biotinylated Goat Anti-Rabbit IgG Antibody (Vector Laboratories BA-1000 lot#: ZF0430) at 1:200 Mouse monoclonal anti-cFVIII (Green Mountain Antibodies, Clone cFVIII 2C4.1C3.F2, monoclonal, lot#: PAB2441; Clone cFVIII 4B1.2C8.B5, monoclonal, Lot#: PAB2417)(Custom made) Rabbit polyclonal anti-cFVIII (Green Mountain Antibodies, GMA153 Lot #HA054) (Custom made)
Validation	Rabbit Anti-human vWF antibodies were validated in-house for ELISA against canine vWF using normal canine plasma. Anti-LRP1 antibodies were validated in-house for Western Blot against canine LRP1 using HA dog liver whole cell lysates. Mouse monoclonal anti-cFVIII antibodies and rabbit polyclonal anti-cFVIII antibodies were validated in-house using recombinant cFVIII proteins, transgenic mouse plasma expressing cFVIII, hemophilia A canine plasma, and normal canine plasma. The other antibodies were validated by the vendor.

Eukaryotic cell lines

Policy information about cell lines

Cell line source(s)	human embryonic kidney cells stably expressing Ad-E4 (ATCC Number: CRL-2784)
Authentication	This cell line was validated to express E4 by immunoblotting in the provided material from ATCC. No additional authentication was performed.

Mycoplasma contamination	Cell line tested negative for mycoplasma contamination.
Commonly misidentified lines (See ICLAC register)	Not applicable.

Animals and other organisms

Policy information about studies involving animals; ARRIVE guidelines recommended for reporting animal research

Laboratory animals	Hemophilia A dogs, 8 males and 1 female, mixed breed, various ages as reported.
Wild animals	Not applicable.
Field-collected samples	Not applicable.
Ethics oversight	All procedures in the dogs were approved by the Institutional Animal Care and Use Committee at the University of North Carolina.

Note that full information on the approval of the study protocol must also be provided in the manuscript.